INTERNATIONAL JOURNAL OF AUTOMOTIVE AND MECHANICAL ENGINEERING (IJAME)
ISSN: 2229-8649 e-ISSN: 2180-1606
VOL. 19, ISSUE 3, 9982 – 9992
DOI: https://doi.org/10.15282/ijame.19.3.2022.10.0770

ORIGINAL ARTICLE

# Deformation Behaviour and Mechanical Response of Closed-cell Cellular Materials under Projectile Impact Using Various Shapes Impactors

M.A. Islam[1,2,*], M.A. Hasib[1], M. Hasan[3] and S. Talapatra[4]

[1]Department of Mechanical Engineering, Khulna University of Engineering and Technology, Khulna 9203, Bangladesh
[2]School of Engineering and Information Technology, UNSW Canberra, ACT-2600 Australia
[3]Industrial & Production Engineering, American International University- Bangladesh, Dhaka-1229, Bangladesh
[4]Department of Industrial Engineering and Management, Khulna University of Engineering & Technology, Khulna 9203, Bangladesh

**ABSTRACT** – Closed-cell cellular materials gained tremendous interest in their application in aerospace, shipbuilding and defence industries due to their exceptional impact energy absorption and lightweight characteristics. To assess the suitability of these materials in practical utilisation, a proper characterisation in dynamic loading is necessary. This paper investigates closed-cell aluminium foam's deformation behaviour due to low-velocity projectile impact in experimentation and finite element analysis. The collapse mechanism was numerically and empirically examined. The experiment and the finite element analysis were found to be in good agreement. The low-velocity projectile impact tests were conducted using an instrumented drop-tower with several projectile tips with an impact energy of 105 J. Finite Element modelling using ABAQUS explicit was undertaken. The results reveal that FE modelling of true foam properties using solid geometry has a good correlation with experimental results. In this study, four impactors/indenters (flat-faced, hemispheric, conical, and truncated-conical) were used. A detailed structural collapse during the low-velocity dynamic impact has been explored with XCT data and finite element tools.

**ARTICLE HISTORY**
Received: 16th May 2022
Revised: 1st Sept 2022
Accepted: 28th Sept 2022
Published: 6th Oct 2022

**KEYWORDS**
*Cellular materials;*
*Finite element modelling;*
*Deformation mechanism;*
*Impact dynamics;*
*Projectile shape*

## INTRODUCTION

Closed-cell metal foams are engineering cellular materials with excellent properties for mechanical applications during impact loading, for example, low-density and high-energy absorption. These properties make them attractive materials for a wide range of applications. Their potential use extends to packaging, automotive, aerospace, military and armour materials [1, 2]. The possible use in defence industries as a sacrificial cladding and kinetic energy absorption of these materials have been assessed in several studies. Most studies have used conventional materials testing machines to examine the response through quasistatic loading [3, 4] or continual velocity loading [5-9]. Also, there is a controversial opinion regarding these materials' inertial and structural sensitivity during impact loading. Some studies claimed that these materials exhibit stain hardening during the impact loading. Islam et al. studied the closed-cell aluminium foams using the Split Hopkinson Pressure Bar [10]. They found that the closed-cell foam exhibits significant strain hardening due to its structural and inertia effects. While there are many studies on the dynamic compaction of these materials, their indention, penetration and perforation behaviour for various shaped projectiles is somewhat inadequate. However, the most typical phenomena these materials are likely to encounter in their working environments include impulsive or collision and confined penetration at low velocity [11-13]. In this regard, there has been very little work done on these materials.

Recently Islam et al. studied the effect of impactors' shape on the mechanical behaviour of closed-cell metal foams experimentally [14]. They used x-ray computed tomography (XCT) to use the deformation of the samples before and after the tests. The XCT-based characterisation of this material is time-consuming and costly. As a result, predicting the impact perforation behaviour of these materials requires a finite element study. Kader et al., as well as other research groups, have used XCT rendered data to simulate and characterise cell collapse using dynamic loading [10, 15-20]. Micro-computed tomography-based foam geometry was used in that work. The results were then explored using ABAQUS/ EXPLICIT. The primary goal of their research was to examine the microstructural collapse of aluminium foams over time. X-ray tomography, on the other hand, is an expensive procedure for evaluating material behaviour for mathematical and empirical inquiry. In this regard, the mechanical and deformation behaviour of the homogeneous geometry of actual foam properties in finite element analysis is intriguing to understand.

In this study, the experimental investigation is conducted to explore the low-velocity impact using several projectile tips. The experimental samples were scanned using XCT before and after the impact to investigate the deformation behaviour. The foam samples were of the same dimension as experimental samples during the finite element analysis. Also, the projectiles were chosen from the sample geometry. After the experimental investigation, all other testing criteria were assigned to the finite element model. The mechanical behaviour and deformation response of empirical and finite

*CORRESPONDING AUTHOR | M.A. Islam | md.islam@me.kuet.ac.bd

element analyses were compared. To understand the deformation mechanisms of the foam for various indenter geometry, we compared the deformation of FE studies with deformation via -CT data.

## MATERIALS AND METHODS

### Materials and Properties

The experimental investigation used CYMAT stabilised aluminium foams (SAFs) with a density of 0.51 g/cc. The foam was made using the direct foaming method [15]. The bulk alloy is melted during foam production. Then, during the manufacturing, stabilised ceramic compounds (SiC/Al2O3) are added to the molten components, which are then put into a foaming box. The bubbles are created by injecting gas (air) into a rotating impeller in a regulated manner, resulting in a foam structure. Variations in operational circumstances, such as gas pressure and temperature, control the cell size. The foundation material was made up of 8-10% silica, 0.5 % magnesium, 1% iron, and 1% copper [15]. A sample of the closed-cell foam that has been tested is given in Figure 1. The foam samples of 1×90 mm were cut from a 500×500 mm and 23 mm thick foam panel. Also, a FE sample of the same dimension as the actual experimental sample is given in Figure 1. Figure 1 depicts a typical macroscopic view of a foam sample and its morphological structure.

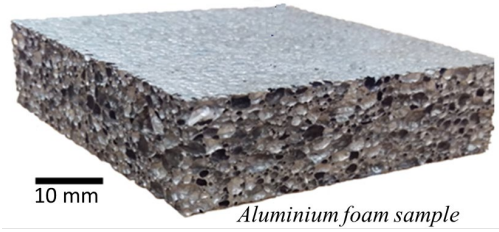


**Figure 1.** A representative sample of closed-cell foam for the low-velocity impact tests.

Low-velocity impact tests were carried out using four different impactors. The experiments were conducted with an automated drop tower (CEAST 9350) fitted with a 90 kN force sensor at an impact velocity of 6 m/s, as illustrated in Figure 2. The test velocity was selected as ~6 m/s so that the impactor does not fully penetrate the specimen to understand the entire deformation field, including underneath the impactor. The total weight of the falling mass was kept at a constant 5.85 kg. The four indenters' geometric profiles are shown in Figure 3.

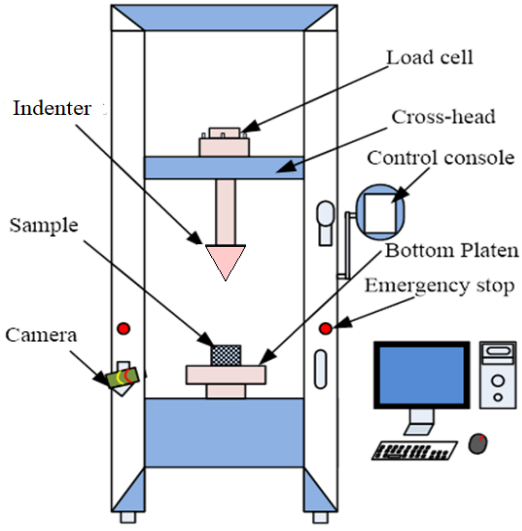


**Figure 2.** Schematic of the drop-weight impact setup.

The impact energies and drop height were adjusted by changing the drop velocities. Samples were attached to a flat hard plate to provide rigid boundary conditions throughout the testing. Furthermore, the impacted specimens were imaged via XCT before and after deformation. Images were captured using a Hamamatsu (Japan) microfocus X-ray source and a flat-screen detector (pixel size: 0.14 m) for imaging. Every degree of rotation of the foam specimen was recorded using radioscopic images. Image indentation images were generated from raw tomography images from the processed medial axis and network generation (MANGO). The raw tomographic images were cleaned using the MANGO software tool's anisotropy diffusion (AD) and unsharp musk (UM) filters. Then the greyscale projections of XCT were transferred to binary images using the MANGO tool.

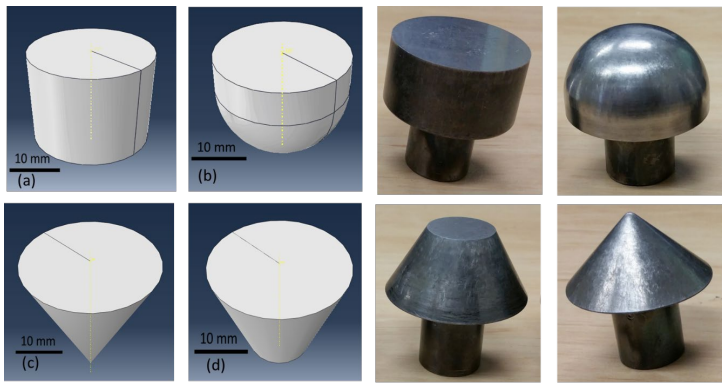


**Figure 3.** Impactor's tips for experimental (right) and numerical (left): (a) flat circular, (b) hemispheric, (c) conical and (d) truncated conical.

## FE Analysis

The target material used for analysis is aluminium foam. A 90 mm square box with a 23 mm thickness serves as the target. The foam's Young's modulus was calculated to be 103 MPa. The Poisson's ratio is assumed to be 0.33. The density of the aluminium foam employed in this project is 530 kg/m3. The Johnson-Cook material model was utilised in the plastic property sections. The Johnson-Cook material model is the most often utilised material model in numerous research studies. A small detail of this material model has been described as follows:

The stress-strain relationship is defined in an equation form in the Johnson-Cook material model. The equation is

$$\sigma = (A + B\varepsilon^n)(1 + C\ ln\ \varepsilon^*)(1 - T^{*m}) \quad (1)$$

where $\sigma$ and $\varepsilon$ are the equivalent Stress and equivalent plastic strain respectively, $A$ , B and C are the constants known as the yield stress of material in reference condition, strain hardening constant, and strengthening coefficient of strain rate respectively, $m$ is the thermal softening coefficient and $n$ is strain hardening coefficient. The values of these material constants are taken from experimental studies [21] as follows: $A$= 324.1 MPa; $B$ = 113.8 MPa; $C$=0.002; $n$ =0.52, $m$ = 1.34 and $\varepsilon_0$ =1.

There is no influence given to temperature measurements in this study. As a result, neither the temperature parameters nor the method for determining all of these values are addressed in this article. Johnson-Cook damage criteria are used in this work. Johnson-Cook Damage equation is stated here:

$$\varepsilon_f = [D_1 + D_2\ exp(\ D_3(\frac{\sigma_m}{\sigma_{eq}}))][1 + D_4\ ln(\ \varepsilon_p{}^*)][1 + D_5 T^*] \quad (2)$$

where $\sigma_m$ is the mean stress, $\sigma_{eq}$ is the equivalent stress, and $D_1$, $D_2$, $D_3$, $D_4$, $D_5$ are the damage model constants, and the value of these constants are taken as -0.77,1.45, 0.47, 0.0, 1.6, respectively. It was assumed that each of the impactors had a distinct rigid body of a different shape. As a result, the primary concern was the impactor's mass. The impactor weighed 5.85 kg, which is considered a point mass.

In the mesh module, the mesh is dependent. For dependent mesh, the parts have meshed in two steps. Part by part, the mesh is done—the approximate global size in the seed option was 1.3 for the target material. In the element library option, explicit is chosen. This target element is of the tetrahedral element type. For this option, C3D4 elements have been chosen. C3D4 means a tetrahedral aspect that has one integration point. C3D4 elements are generally used for solving any structural element analysis. A total of ~5500 elements produced the best results for the optimum computational time.

The approximate global size in the seed option was 0.8 for the target material. The stiff impactor has R3D4 elements attached to it. A gravity load is applied in the load module. In boundary condition sections, the target material's exterior faces are considered encastre, which means no movement or rotation exists for all these four faces. In the base face of the target material, displacement or rotation type is selected. Only vertical or translational motion is permitted within this boundary condition.

For the impactor, a boundary condition is imposed in the reference point upon which the weight of the impactor acts. In this reference point, the boundary condition type is displacement or rotation. Furthermore, this boundary condition only permits movement in the vertical direction. In the predefined field manager command, an initial velocity is defined in the reference point. Different velocities are assigned for the detailed analysis of this dynamic problem.

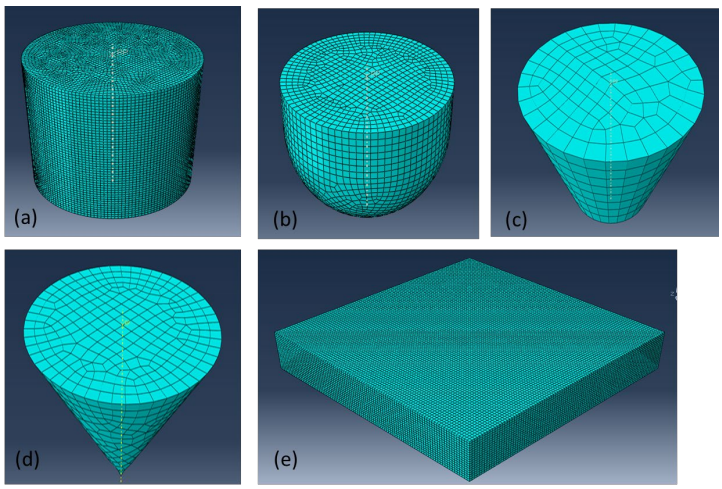


**Figure 4.** Meshed geometry of the impactors and target foam sample.

## EXPERIMENTAL RESULTS

At first, the quasistatic compression and dynamic compression tests of the foam samples were carried out to evaluate the mechanical behaviour of the foam in static loading. The assessments were carried out using conventional UTM (Shimadzu AGX V-series) with a strain rate of $10^{-3}$ $S^{-1}$. On the other hand, dynamic compression tests were carried out using a drop tower with an impact velocity of 6 m/s. The stress-strain curves in quasistatic and dynamic compaction tests are shown in Figure 5. The quasistatic specimens were compressed to approximately 12 mm (~50% of nominal strain).

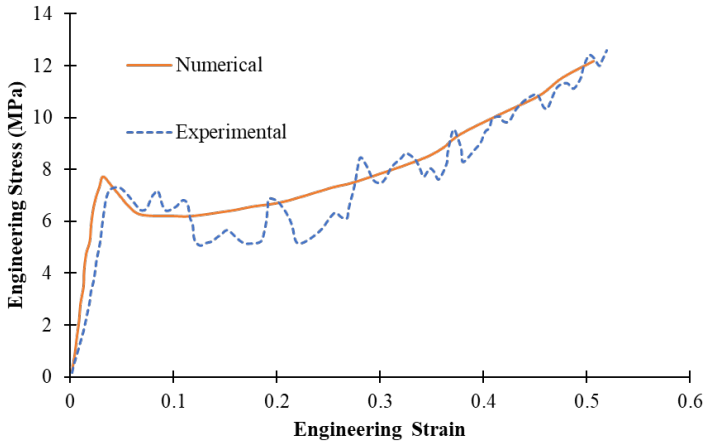


**Figure 5.** The stress-strain curves of closed-cell aluminium foams during quasistatic (QS) and impact (drop weight) tests.

The stress-strain curves from drop-tower loading exhibit oscillations, as may be shown in Figure 5. This was most likely due to the specimen and impactor interacting in a repeated wave pattern. As a possible explanation for the oscillation, cycles of plastic collapse in the sample's weaker regions could be to blame. [23, 24] reported similar oscillations in the dynamic loading of similar materials.

Low-velocity indention and impact tests were carried out with the same drop tower machine with customised projectile tips such as flat-circular, hemispheric, conical and truncated-conical. The response of the load-displacement curve with the variation of impact for individual indenters is also shown in Figure 6 and Figure 7. The load-displacement curves of finite element analysis are also presented with the experimental load-displacement curve. It is noted that the load-displacement curve for the flat-circular indenter has higher oscillation than all other indenters. The oscillation during the impact was the wave interaction between the indented and the target. The cross-sectional area of the conical indenter gradually increased as the depth of indentation increased. Crushing and frictional forces were increased in the specimen's inclined indentation due to the impact, which led to an increasing load. At the beginning of the curve, the truncated-conical indenter shows an interesting curve that has the effect of a flat and conical indenter combined. It is presumed that the actual impact was caused by a combination of foam crushing beneath the indenter, tearing, and frictional work (discussed in a later section). Overall, a good agreement between the experimental and FE load-displacement curve is found for all the indenters.

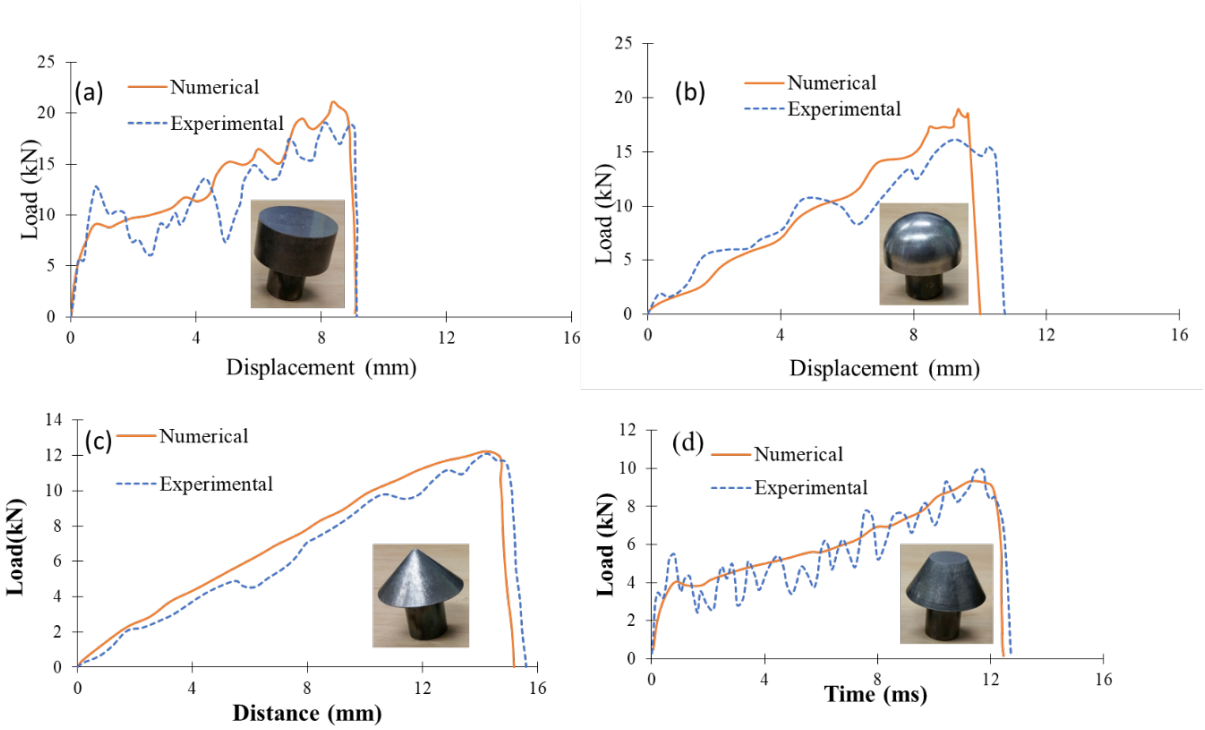


**Figure 6.** Load-indentation depth curves for four different shaped indenters.

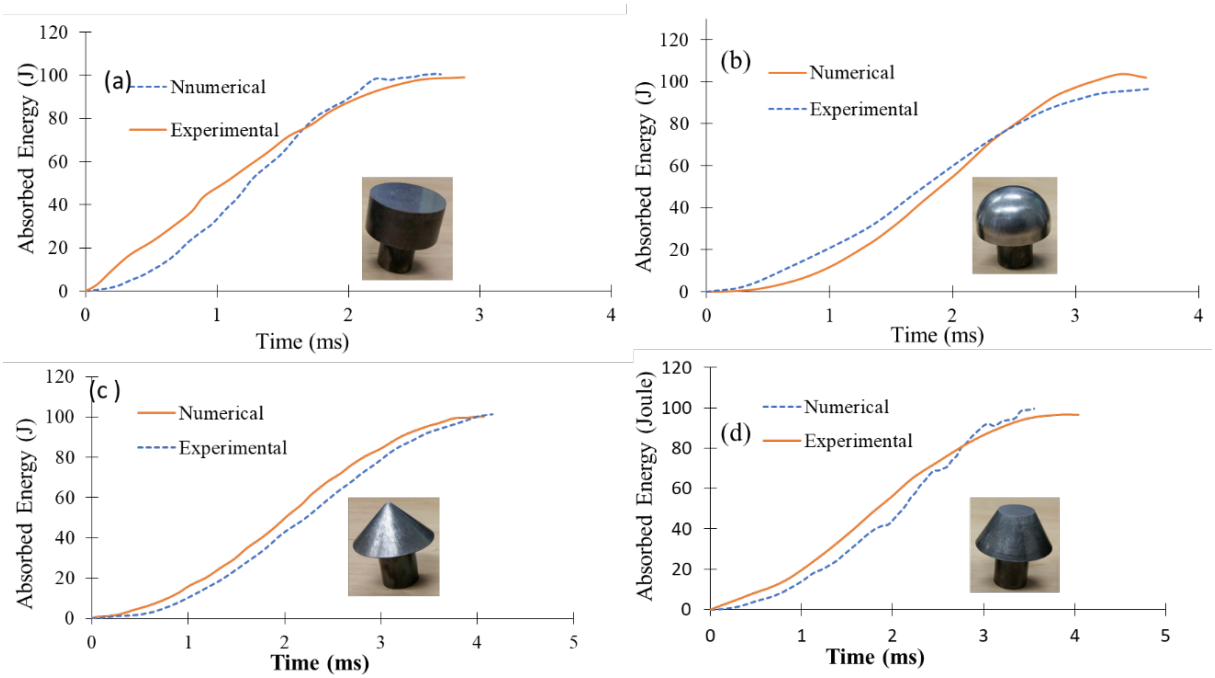


**Figure 7.** Energy absorption curves for four different shaped indenters.

The response of dynamic indentation in the foam samples for all four indenters are further evaluated for the impact energy absorption capacity for various indenters during impact. The energy dissipation of the foam samples due to the impactor for experimental and FE analysis are also presented in Figure 7. It is noted that the impact reaction time for the flat-circular indenter is the shortest, whereas the reaction time of the conical indenter is noted highest. The overall trend of the FE and experimental curves for all the indenter has a good agreement. The variation of the load-displacement graph between experimental and numerical curves lies within 5-7%. The energy absorption curve of the experimental and numerical has a good agreement.

Energy absorption can be estimated from the force-displacement curve. In addition, the total energy absorption and absorption efficiency for the flat-circular indenter are as follows [21]:

$$\text{Energy absorption, } W = \int_0^{\varepsilon} \sigma(\varepsilon) d\varepsilon \tag{3}$$

Energy absorption efficiency:

$$\eta(\varepsilon) = \frac{1}{\sigma(\varepsilon)} \int_0^{\varepsilon} \sigma(\varepsilon) d\varepsilon \tag{4}$$

The velocity attenuation has further evaluated the characterisation of foams resistance to indentation. The velocity attenuation over time can be regarded as the energy dissipation by the indenters. The profile of velocity attenuation for the indenters has a good fit with the model as reported in [12, 13, 22]:

$$V(t) = \left\{ V_0^2 - \frac{2\sigma_{cr}}{\rho_0} \ln\left(1 - \frac{x}{\varepsilon_D \vartheta}\right) \right\}^{1/2} \tag{5}$$

The resistance forces of the foams for the indenters have been analysed from the relationship between applied forces, reaction forces and amount of deformation. The analysis of all four indenters can be evaluated by applying Newton's second law of motion.

According to the second law:

$$m\frac{dv}{dt} = -F_d \tag{6}$$

The dynamic perforation force acting on the foams sample can be expressed as crushing the foams beneath the indenter and tearing the call around the edge of the indenter.

$$F_d = F_{crush} + F_{tear} + F_{Friction} + F_{Shock} \tag{7}$$

Now, for the flat circular indenter, the penetration resistance load by the foam specimen excluding the shock wave effect for our low-velocity tests as the crushing, friction and tearing forces.

$$F_p = F_{crush} + F_{Tearing} \tag{8}$$

The frictional force between the flat indenter surface and the foam is minimal since the deformation is localised underneath the indenter. Thus, the tearing of the cell wall and the crushing of the cell wall would be considered the total force. Hence, the indenter resistance force $F_d$ is expressed as:

$$F_d = \pi r^2 \sigma_{pl}^* + 2\pi r \Gamma \tag{9}$$

$$\Gamma = (F_d - \pi r^2 \sigma_{pl}^*)/2\pi r = \frac{(p_d - \sigma_{pl}).r}{2} \tag{10}$$

where, $p_d = \frac{F_d}{\pi r^2}$ , Where $p_d$ is the plateau stress in the quasistatic test and $r$ is the indenter's radius. From the experimental data of the closed-cell of 0.51 g/cc density foam, the $\Gamma$ value has been calculated from the quasistatic indentation tests, which was found as 18.6 kJm$^{-2}$. The tearing energy can be further estimated by [22] as:

$$\Gamma = C\left(\frac{\rho_f}{\rho_s}\right)^n \text{ kJm}^{-2}$$

Now, for the hemispheric indenter total resisting force,

$$F_d = F_{tear} + F_{crush} + F_{Friction} \tag{11}$$

$$F_d = \frac{\pi D^2 \sigma_{pl}}{4} + \pi D\Gamma + \pi D\mu_d \tag{12}$$

In the case of truncated indenter, the plastic cell collapse occurred directly beneath the flat part and of the indenter and tearing of cell contact between the indenter's slant surfaces as the indenter moves deeper into the specimen. Thus, the indentation for a truncated indenter comprises plastic crushing energy and tearing the cell by the slant surface and the force required to shear the slant surface as the indenter is pushed into the specimen [8]. According to [23], the resistance force can be calculated by:

$$F_d = F_{crush} + F_{tearing} + F_{shear} \tag{13}$$

$$F_d = F_c + F_t + F_s/\cos\ \theta \tag{14}$$

$$F_d = \sigma^* \pi r^2 + 2\pi r\Gamma + \frac{\tau^*}{\cos\theta}\pi h(h\tan\theta + 2r) \tag{15}$$

where, r is the radius of the indenter tip (10 mm for the truncated indenter and 2mm for the conical). $\sigma^*$ is the yield stress of the foam estimated as ~5 MPa during quasistatic compression.

## DEFORMATION ANALYSIS

The deformation of the experimental specimens has been investigated using X-ray μ-CT data analysis. At first, the compressed samples in drop weight loading were elucidated. A representative sample after reconstruction of 3D image from XCT data and post-processing of finite element sample are shown in Figure 8. DRISHTI is used to recreate indented specimens using X-ray computed tomography data and 3D image analytics.

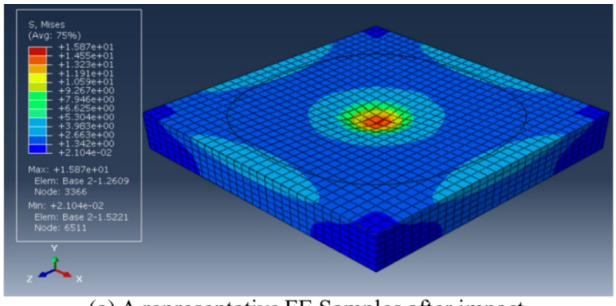


(a) A representative FE Samples after impact

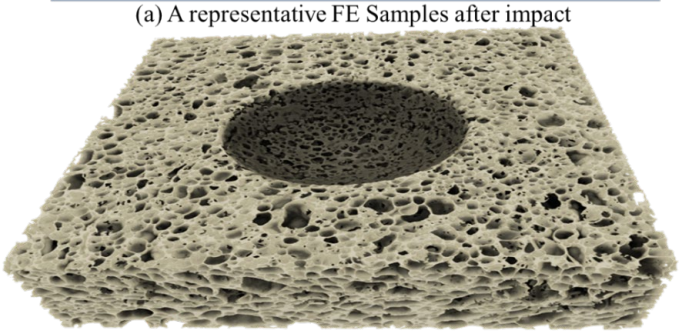

(b) A reconstructed experimental sample after impact

**Figure 8.** A representative post-impact numerical and experimental sample impacted by a hemispheric impactor.

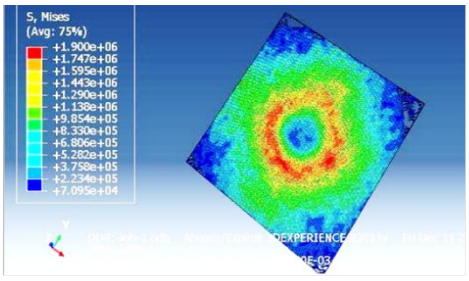


(a) Plane transverse to loading ( Numerical)

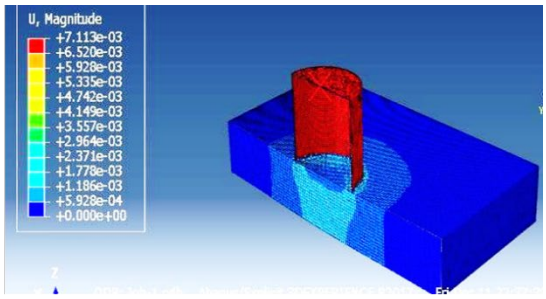


(b) Plane transverse to loading ( Numerical )

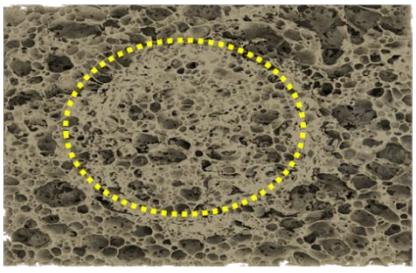

(c) Plane transverse to loading ( Experimental)

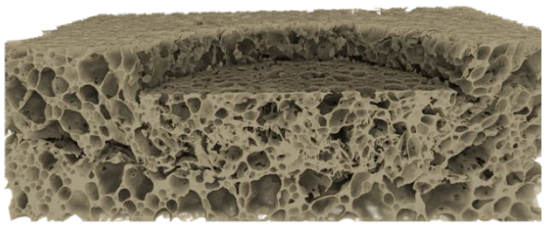

(d) Plane parallel to loading ( Experimental )

**Figure 9.** Cells collapse field of closed-cell metal foam of experimental and finite element sample stuck by a flat-circular indenter: (a) a section perpendicular to the loading direction, (b) a section parallel to the loading direction, (c) a section perpendicular to the loading direction for FE sample, and (d) a section parallel to the loading direction for FE sample.

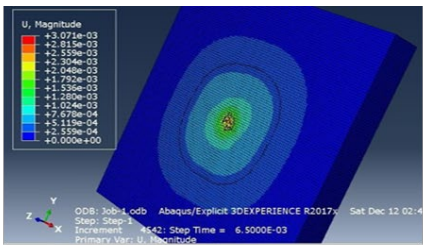


(a) Plane transverse to loading (Numerical)

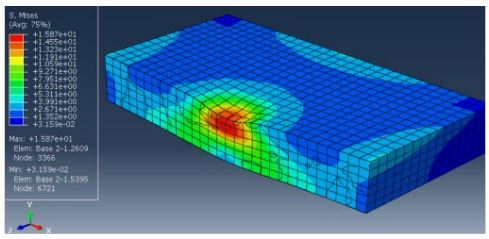


(b) Plane parallel to loading (Numerical)

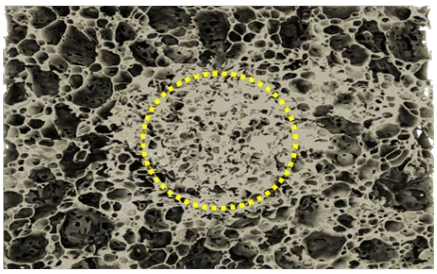

(c)Plane transverse to loading (Experimental)

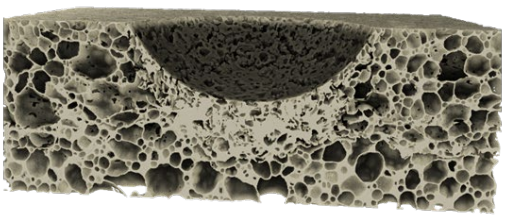

(d) Plane parallel to loading (Experimental)

**Figure 10.** Cells collapse field of closed-cell metal foam of experimental and finite element sample stuck by a hemispheric indenter: (a) a section perpendicular to the loading direction, (b) a section parallel to the loading direction, (c) a section perpendicular to the loading direction for FE sample, and (d) a section parallel to the loading direction for FE sample.

The deformation fields of internal sections of indented materials affected in experiments and FE analysis are shown in Figure 9 to Figure 12. Each figure depicts various inside views of the indented samples, such as a 3D cross-section and a crosswise section. Both finite element and reconstructed XCT samples show that there is little distortion or deformation in the surrounding area of the sample, and the indentation is localised underneath the indenters. The same results were noticed for the other indenters types for experimental and FF samples.

Post-processing FE samples further elucidate the deformation field of indented specimens for all four indenters. During the deformation, the collapse was observed to begin just below the impactors' surface, just like in the experimental samples. The impact force beneath the indenter was totally absorbed by the collapsing cells. The hemispheric, conical, and truncated-conical indenters have a similar deformation field, with the deformations being much more confined beneath the indenters. The deformation field of real samples is shown to be in good agreement with the deformation field in FE analysis. As a result, using the FE analysis in this work, equivalent research using different indenters can be predicted. Because no more material deterioration is necessary, this FE analysis may be more sustainable than the experimental study.

Visualisations based on XCT data demonstrated clearly the specimen's deformation process. Figure 9 to Figure 12 show that deformation spread from the impactor surface to the specimen's bottom as the indenter descended into the foam. Foam XCT data has also been examined in a transverse section to investigate mechanisms of lateral deformation. Even though the mesoscale strain was massive, there was no global strain at all because the cell walls from the top filled the neighbouring voids (cell level). Frictions between adjacent cell walls in a small area can increase the amount of energy absorbed. On the other hand, the specimens' bottoms show no signs of deformation in any of the indentation tests. In low-velocity projectile impact environments, this indicates that closed-cell aluminium foam can be used as an impact energy absorber, such as in sacrificial cladding or protective shields, and can reduce damage to the rear of the foam sample if it is thick enough.

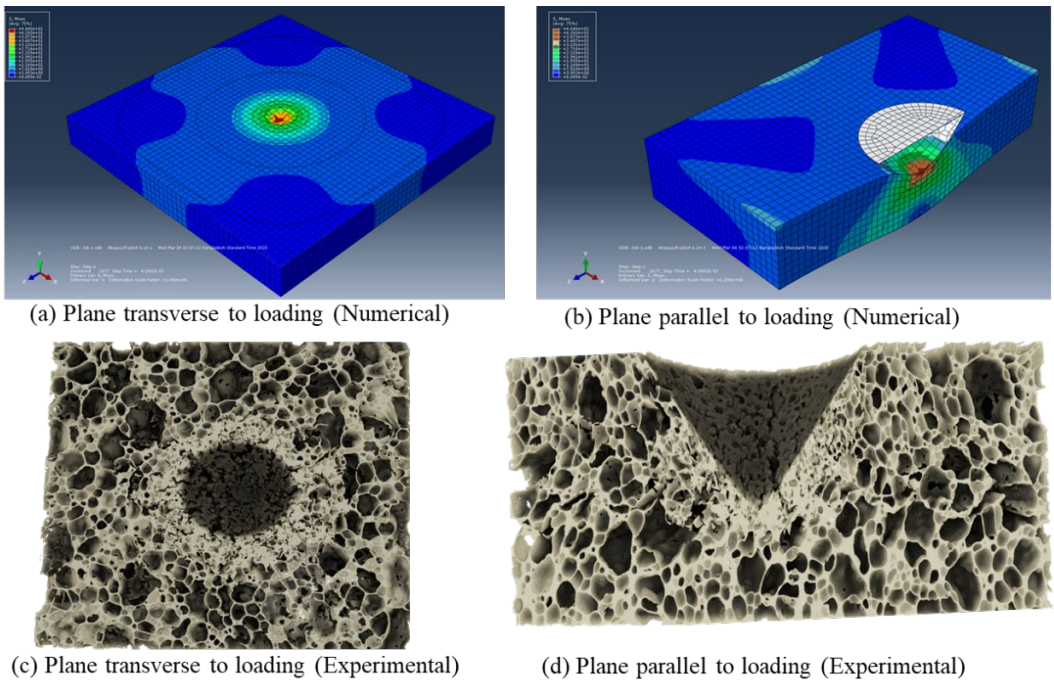

(a) Plane transverse to loading (Numerical) (b) Plane parallel to loading (Numerical)

(c) Plane transverse to loading (Experimental) (d) Plane parallel to loading (Experimental)

**Figure 11.** Cells collapse field of closed-cell metal foam of experimental and finite element sample stuck by a conical indenter: (a) a section perpendicular to the loading direction, (b) a section parallel to the loading direction, (c) a section perpendicular to the loading direction for FE sample, and (d) a section parallel to the loading direction for FE sample.

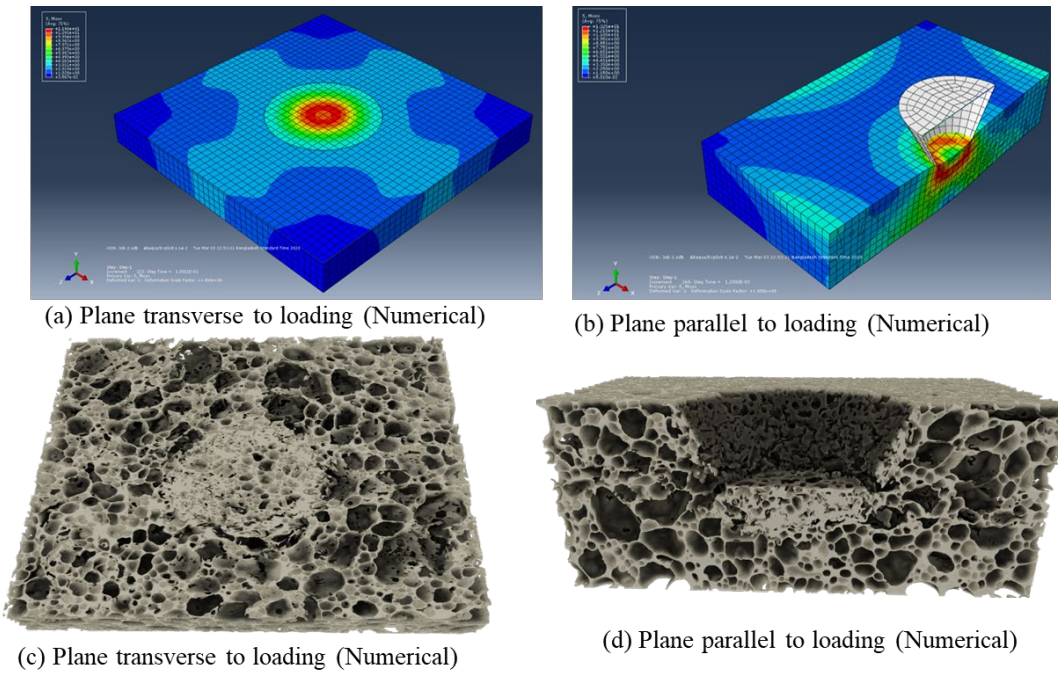

(a) Plane transverse to loading (Numerical) (b) Plane parallel to loading (Numerical)

(c) Plane transverse to loading (Numerical) (d) Plane parallel to loading (Numerical)

**Figure 12.** Cells collapse field of closed-cell metal foam of experimental and finite element sample stuck by a truncated-conical indenter: (a) a section perpendicular to the loading direction, (b) a section parallel to the loading direction, (c) a section perpendicular to the loading direction for FE sample, and (d) a section parallel to the loading direction for FE sample.

Overall, the experimental and FE deformation of closed-cell foam under low-velocity impact using various indenters are summarised in Figure 13. The foam adjacent to the indenter surface deformed first. This deformed foam pushed into the foam as the indenter further went until the foam absorbed the total kinetic energy of the indenter through deformation. Finally, the foam's entire deformation zone under the indenter makes a shape almost similar to the indenters' outer shape that penetrated the foams. Deformed cell walls migrated toward nearby void spaces and then bent based on the shape of the voids, as shown in this experiment (Figure 9 to Figure 12). Figures 9 to Figure 12 show that the top wall of pores moves toward the voids by forming hinges at weaker points. Most pore collapse occurs just beneath indenters; the cells at the bottom, on the other hand, remain unaltered. Consequently, the deformation of the foam area is highly localised, and almost all of the impact energies of the impactor are absorbed by the foam adjacent to the impactor. This implies that

these materials are appropriate for impact energy absorbent in armour materials and sacrificial cladding in armour vehicles.

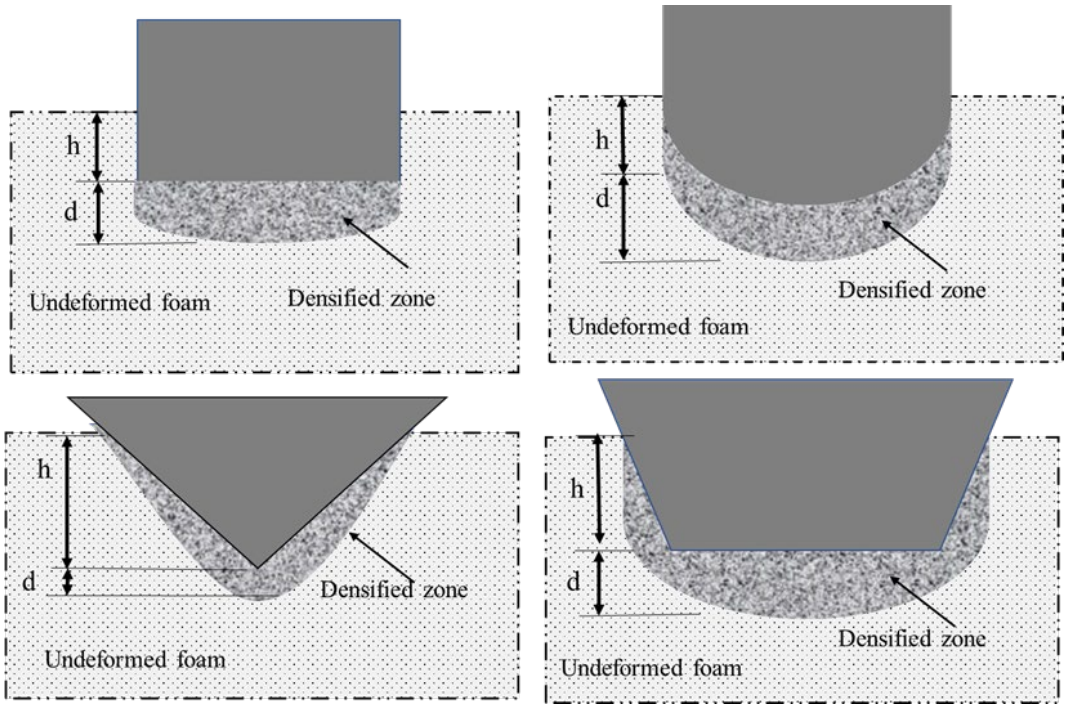


**Figure 13.** A summary of closed-cell foam deformation during experimental and numerical analysis.

## CONCLUSION

The mechanical performance of closed-cell aluminium foams was examined using low-velocity impact testing and FE modelling. XCT data rendering and FE analyses were also used to study the collapse behaviour of closed-cell foams under low-velocity impacts. Dynamic indentation testing has investigated the cell collapse mechanisms and energy absorption capacity of CYMAT closed-cell aluminium metal foams. The XCT reconstructed foam geometry and FE post-processing samples were explored to elucidate the detailed structural deformation. The following specific conclusions can be drawn from the current investigation:

i. The FE study of closed-cell foams employing experimental material parameters into a homogenous material model shows that the mechanical behaviour and deformation field are similar to those seen in the experimental inquiry.
ii. XCT of the impacted samples (drop impact) showed that the collapse field in low-velocity impact commenced just beneath the indenter (Figure 19 to Figure 13) and spread with the indenters until the foams' resistance fully stopped the impactors.
iii. Closed-cell aluminium foam's response to low-velocity impacts is influenced by the shape of the indenter's nose and the preliminary impact energy at which the impact occurred, according to experimental results.
iv. For both experimental and FE, the load-displacement and absorbed energy-time graphs show a similar pattern. As a result, it is clear that FE analysis employing continuum geometry with actual foam properties produces results that are comparable to those obtained in the experimental work.
v. The cell collapse of the foams began right beneath the indenter (see Figure 9 to Figure 12) and propagated with the indenters, according to the study (both experimental and FE).

## ACKNOWLEDGEMENT

The authors warmly recognise the material testing facilities at UNSW Canberra in Canberra, Australia, for their assistance with materials testing.

## REFERENCES

[1] L.J. Gibson, M.F. Ashby, and BA. Harley, *Cellular materials in nature and medicine*, Cambridge: Cambridge University Press, 2010.
[2] L.J. Gibson, and M.F. Ashby, *Cellular solids: structure and properties*, Cambridge: Cambridge University Press, 1999.
[3] A. Brown *et al.*, "Effects of thermal processing on closed-cell aluminium foams," in *Characterisation of Minerals, Metals, and Materials*. S. Ikhmayies, B. Li, J.S. Carpenter, J. Li *et al.*, Eds. Cham: Springer. pp2017, 217-224, doi: 10.1007/978-3-319-51382-9_24.
[4] Elnasri, I. and H. Zhao, "Impact perforation of aluminium Cymat foam," *Int. J. Mech. Sci.*, vol. 150, pp. 79-89, 2019, doi: 10.1016/j.ijmecsci.2018.10.016.

[5] Olurin, O.B., NA. Fleck, and M.F. Ashby, "Indentation resistance of an aluminium foam," *Scripta Materialia*, vol. 43, no.11, pp. 983-989, 2000, doi: 10.1016/S1359-6462(00)00519-4.

[6] Sun, Y. and QM Li, "Dynamic compressive behaviour of cellular materials: A review of phenomenon, mechanism and modelling," *Int. J. Impact Eng.*, vol. 112 (Supplement C), pp. 74-115, 2018, doi: 10.1016/j.ijimpeng.2017.10.006.

[7] M.A Yahaya, D. Ruan, G. Luc, and M.S. Dargusch, "Response of aluminium honeycomb sandwich panels subjected to foam projectile impact – An experimental study," *Int. J. Impact Eng.*, vol. 75: pp. 100-109, 2015, doi: 10.1016/j.ijimpeng.2014.07.019.

[8] Y. Fei *et al.*, "Experimental and numerical studies of the anti-penetration performance of sandwich panels with aluminum foam cores," *Acta Mechanica Solida Sinica*, vol. 28, no.6, pp. 735-746, 2015, doi: 10.1016/S0894-9166(16)30013-1.

[9] Zhao, H., I. Elnasri, and S. Abdennadher, "An experimental study on the behaviour under impact loading of metallic cellular materials," *Int. J. Mech. Sci.*,. vol. 47, no. 4–5, pp. 757-774, 2005, doi: 10.1016/j.ijmecsci.2004.12.012.

[10] Kader, M.A., et al., Strain-rate dependency and impact dynamics of closed-cell aluminium foams. Materials Science and Engineering: A, vol.?, p. 141379, 2021.

[11] Kumar, P.S., et al., *Effect of displacement-rate on the indentation behavior of an aluminum foam.* vol. 347, no.1-2, pp. 330-337, 2003.

[12] S. Ramachandra, P.S. Kumar, and U. Ramamurty, "Impact energy absorption in an Al foam at low velocities," *Scripta Materialia*, vol. 49, no.8, pp. 741-745, 2003, doi: 10.1016/S1359-6462(03)00431-7.

[13] U. Ramamurty, and M.J.A.M Kumaran, "Mechanical property extraction through conical indentation of a closed-cell aluminum foam," *Acta Materialia*, vol. 52, no.1, pp. 181-189, 2004, doi: 10.1016/j.actamat.2003.09.004.

[14] M.A. Islam *et al.*, "*Mechanical response and dynamic deformation mechanisms of closed-cell aluminium alloy foams under dynamic loading,"* vol. 114, pp. 111-122, 2018.

[15] M.A. Kader *et al.*, "Deformation mechanisms of closed cell-aluminium foams during drop weight impact," in *Characterisation of Minerals, Metals, and Materials*, S. Ikhmayies, B. Li, J.S. Carpenter, J. Li *et al.*, Eds. Cham: Springer, 2017, p. 233-239, doi: 10.1007/978-3-319-51382-9_26.

[16] M.A. Kader *et al.*, "Modelling and characterisation of cell collapse in aluminium foams during dynamic loading," *Int. J. Impact Eng*.,.vol. 96: pp. 78-88, 2016 doi: 10.1016/j.ijimpeng.2016.05.020.

[17] M.A. Kader *et al.*, "Macro and micro collapse mechanisms of closed-cell aluminium foams during quasistatic compression," *Mater. Des.,* vol.18, pp. 11-21, 2017, doi: 10.1016/j.matdes.2017.01.011.

[18] M.A. Kader, M.A. Islam, P.J. Hazell, and J.P. Escobedo, "Computational modelling of closed-cell aluminium foams to investigate structural deformation under quasistatic loading," in *Appl. Mech. Mater.,* vol. 846, pp. 133-138, 2016, doi: 10.4028/www.scientific.net/AMM.846.133.

[19] N. Khaire, V. Bhure, and G. Tiwari, "Finite element analysis of impact response of foams in sandwich panels," *Materials Today: Proceedings*, vol. 28, pp. 2585-2590, 2020, doi: 10.1016/j.matpr.2020.05.703.

[20] Z.H. Tan, H.H. Luo, W.G. Long, and X. Han, "Dynamic response of clamped sandwich beam with aluminium alloy foam core subjected to impact loading," *Compos. B. Eng.*, vol.46, pp. 39-45, 2013, doi: 10.1016/j.compositesb.2012.10.044.

[21] M.A. Islam *et al.*, "Investigation of microstructural and mechanical properties of cell walls of closed-cell aluminium alloy foams," *Mater. Sci. Eng.*: A, vol. 666, pp. 245-256, 2016, doi: 10.1016/j.msea.2016.04.046.

[22] P. S. Kumar, S. Ramachandra, and U. Ramamurty, "Effect of displacement-rate on the indentation behavior of an aluminum foam," *Mater. Sci. Eng.,* A,.vol. 347, no.1–2, pp. 330-337, 2003, doi: 10.1016/S0921-5093(02)00608-1.